catalysts

MDPI

Article

Supported Ionic Liquid Catalysts for the Oxidation of S- and N-Containing Compounds—The Effect of Bronsted Sites and Heteropolyacid Concentration

Vladislav Gorbunov [1], Aleksey Buryak [2], Kirill Oskolok [1], Andrey G. Popov [1] and Irina Tarkhanova [1,*]

[1] Department of Chemistry, Lomonosov Moscow State University, 119991 Moscow, Russia
[2] A.N. Frumkin Institute of Physical Chemistry and Electrochemistry, Russian Academy of Sciences, 31-4 Leninsky Prospect, 119071 Moscow, Russia
* Correspondence: itar_msu@mail.ru

Abstract: In this article, a series of effective catalysts based on betaine and sulfuric or phosphomolybdic acids was obtained. These compositions were characterized by various physicochemical methods and tested in the oxidation of sulfur- and nitrogenous-containing compounds by H_2O_2. An increase in the amount of heteropolyacid (HPA) leads to a non-linear change in acidity, and the degree of removal of sulfur-containing compounds correlates with the concentration of Bronsted acid sites on the surface. On the contrary, the degree of pyridine removal is determined primarily by the content of heteropolyacids in the catalyst.

Keywords: desulfurization; denitrogenation; ionic liquids; polyoxometalates

Citation: Gorbunov, V.; Buryak, A.; Oskolok, K.; Popov, A.G.; Tarkhanova, I. Supported Ionic Liquid Catalysts for the Oxidation of S- and N-Containing Compounds—The Effect of Bronsted Sites and Heteropolyacid Concentration. *Catalysts* **2023**, *13*, 664. https://doi.org/10.3390/catal13040664

Academic Editors: Eduard Karakhanov and Aleksandr Glotov

Received: 1 March 2023
Revised: 24 March 2023
Accepted: 26 March 2023
Published: 28 March 2023

1. Introduction

The ever-increasing demand for fossil fuels leads to higher amounts of hazardous emissions, which pollute the environment. Therefore, requirements for the quality of oil-derived products increase from year to year. Fuel combustion produces nitrogen- and sulfur-containing compounds and carbon monoxide, which are released into the atmosphere. For this reason, a goal pursued by many researchers is to find a way to minimize harm to the environment by thorough purification of fuel from toxic compounds. Nitrogen and sulfur compounds are adverse to the environment and human health. The amount of residual sulfur has been strictly regulated since long ago [1,2], but this is not the case for nitrogen compounds. A quantitative restriction of the nitrogen oxide emission for diesel engines of light motor vehicles was introduced only recently [3–5]. It is commonly known that hydrogenation is the key industrial process used to remove sulfur compounds from oil products [6]. However, as the molecular weight of the sulfur substrate increases, more drastic conditions are required for this process [7] to increase efficiency. Therefore, in some cases, hydrogenation can be replaced by alternative hydrogen-free processes [8], in particular, catalytic oxidation using hydrogen peroxide, which is easy to implement and environmentally friendly [9,10].

The catalysts used for desulfurization include Brønsted acids and ionic liquids (ILs) with acid sites and derivatives of some transition metals, in particular, polyoxometalates [11,12].

It is efficient to combine catalytic oxidation with the subsequent removal of products by extraction or adsorption. The oxidation products are more polar than the initial heteroatomic compounds and more so than fuel hydrocarbons; hence, they can be extracted with organic polar solvents [13] or with ionic liquids [14,15].

The adsorption removal of sulfur compounds and their oxidized derivatives is based on extraction caused by selective interaction between the adsorbate molecules and the adsorbent surface. The commonly used adsorbents are solid metal-organic frameworks [16–18], nanocomposites [19], organic polymer supports [20], and active carbon-based fibers [21].

A promising method is to remove heteroatomic compounds from oil distillates using ionic liquids as catalysts or extractants, owing to their unique properties and variable structure [22–24].

The most interesting approach is to use ionic liquids simultaneously as catalysts of hydrogen peroxide oxidation and as extractants for sulfur compounds [25,26].

The question arises of what criteria should be used to select the appropriate catalyst for a particular oxidation reaction of sulfur compounds. It was found that the strength and the type of acid sites in the catalysts are one of the most important criteria [27]. Systems are effective if their acidity is provided by a sulfonic acid ($^{-}SO_3H$) linked by a covalent bond to the organic cation of IL and by a Brønsted acid counter-ion, hydrogen sulfate (HSO_4^{-}), or dihydrogen phosphate ($H_2PO_4^{-}$) [28].

Although the recycling techniques for these compositions are known [29], immobilization of the catalytically active component on the adsorbent surface to obtain supported ionic liquids (SIL) is appropriate to decrease IL consumption and facilitate the catalyst recovery [30].

Oxidative desulfurization supplemented by extraction or adsorption is a promising technique. The ILs that have active sites in both cation and anion moieties are the most efficient catalysts. For example, the cation may contain a Brønsted acid site, and the anion may contain a polyhydric acid residue of phosphoric, sulfuric [31], or phosphomolybdic, phosphotungstic acid, which form peroxo complexes upon reactions with oxidants [12,32]. The fabrication of these complex polyfunctional heterogeneous compositions gives rise to catalysts that are active and stable in oxidative desulfurization.

Nitrogen compounds poison hydrotreating catalysts; therefore, in some cases, their presence requires additional steps in the process [33].

The nitrogen compounds present in oils are subdivided into basic (pyridine derivatives) and non-basic (pyrrole derivatives). Oil hydrotreating can convert non-basic nitrogen compounds to strong bases before amine is eliminated as ammonia [34].

Catalytic hydrogenation is most often used in industry to remove nitrogen from oils. Among heteroatomic compounds present in oil feedstock (S, N, and O), nitrogen compounds are the most difficult to eliminate by this method. This is especially true for pyridine nitrogen. The influence of nitrogen compounds on oxidative desulfurization for various catalysts was studied. For example, the presence of quinoline and indole does not affect oxidative desulfurization, while pyrrole and pyridine decrease the rate of thiophene removal in the oxidation with H_2O_2 [33].

Here we studied the catalytic compositions obtained from 4-(3′- ethylimidazolium) butanesulfonate (betaine) derivatives and containing two types of catalytically active sites, Brønsted sites, due to protonation of betaine with sulfuric or phosphomolybdic acid (PMA) (see Figure 1), and oxometalate sites.

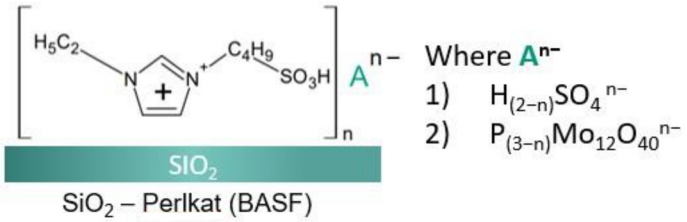

Figure 1. The composition of the obtained catalysts.

The catalysts were deposited on a solid adsorbent, silica gel. The catalysts were tested in the hydrogen peroxide oxidation of model substrates, dibenzothiophene, thioanisole, and pyridine, taken as examples of heteroatomic components of diesel fractions [35]. In addition, we used thiophene, which is present in light oil fractions and is the heterocyclic compound most difficult to oxidize [30].

A significant factor for these catalytic systems is the number and type of acid sites; therefore, the purpose of this study was to elucidate the effect of the Brønsted acidity and

the content of heteropolyacid on the catalytic properties of samples towards the oxidation of test substrates with hydrogen peroxide.

2. Results and Discussion

2.1. Physico-Chemical Characteristics of the Synthesized Ionic Liquids and Heterogeneous Catalysts

Figure 2 shows the IR spectra of $H_3PMo_{12}O_{40}$, betaine, and their derivative (PMoIL1) in the frequency ranges of 500–1800 and 500–900 cm^{-1}, and oxometalate sites.

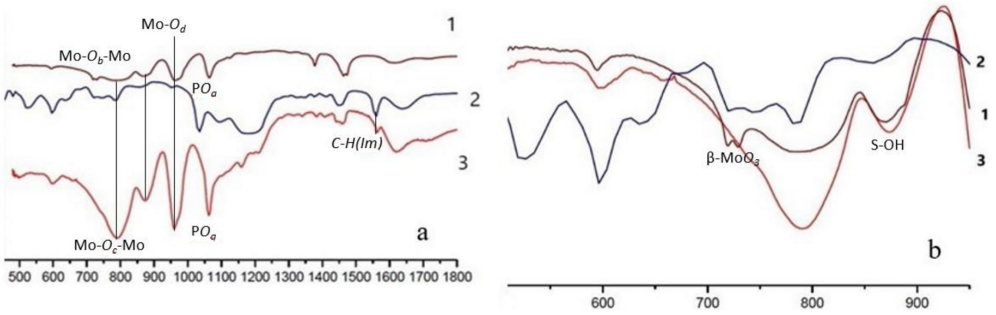

Figure 2. IR spectra (1)—$H_3PMo_{12}O_{40}$; (2)—4-(3′-ethylimidazolium)-butanesulfonate; (3) PMoIL1 in the range (**a**) 500–1800 (**b**) 500–900 cm^{-1}.

Spectra 1 and 3 show absorption bands for the PMo12O40 heteropolyanions. The P-O bond gives rise to a characteristic band at 1064 cm-1 (vas POa). The bands at 960, 872, and 789 cm^{-1} correspond to the vas Mo-Od, vas Mo-Ob-Mo, and vas Mo-Oc-Mo modes. The 1560 cm-1 band present in the spectrum belongs to the stretching vibrations of the imidazolium moiety (1600–1500 cm^{-1}).

According to published data [36], the decomposition of the acid produces two additional weak bands at 775 cm^{-1}, which can be attributed to monoclinic molybdenum oxide (beta- MoO_3). In spectrum 3, there are no such bands; this means that the heteropolyanion structure is retained after interaction with betaine. Apart from the band at 872 cm^{-1} (v_{as} Mo-O_b-Mo), spectrum 3 (Figure 2b) shows absorption at 880 cm^{-1}, which can be assigned to S-OH vibrations of the SO_3H group in sulfonic acids [37]. Thus, from analysis of the spectra, it can be seen that the sulfo group is protonated by the heteropolyacid.

Figure 3 shows micrographs of PMo1 catalyst samples and element distribution maps for S, P, and Mo.

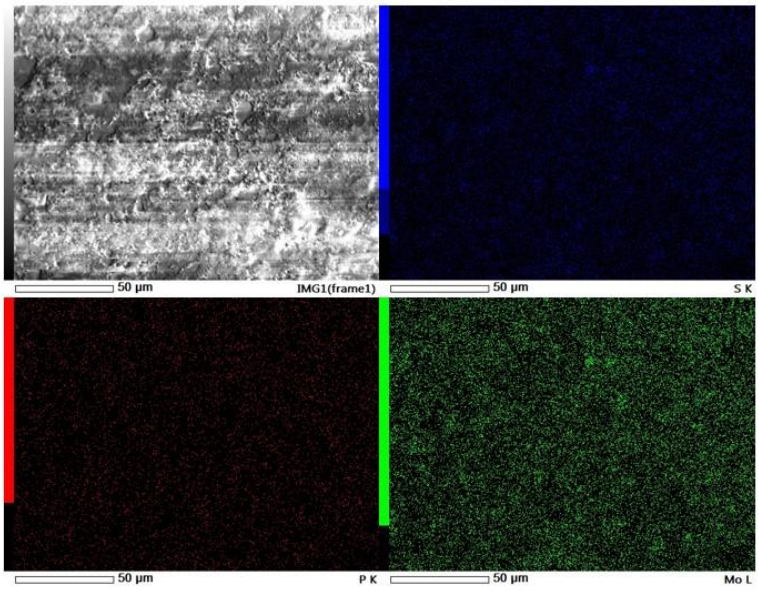

Figure 3. SEM micrograph and distribution of sulfur, phosphorus, and molybdenum on the surface of the PMo1 molybdenum catalyst.

Analysis of the micrographs indicates that the coatings are dense and continuous and that the location areas of S and Mo coincide. Table 1 presents the element distributions on the PMo1 catalyst surface according to EDA data.

Table 1. Distribution of elements on the PMo1 surface according to EDA data.

Element	(keV)	Weight, %	Sigma	Atom, %	K
C K	0.277	16.13	0.18	23.23	3.06
N K	0.392	5.94	0.24	7.36	4.67
O K	0.525	52.00	0.37	56.22	43.59
Si K	1.739	19.49	0.11	12.00	38.16
P K *	2.010	0.04	0.02	0.02	0.07
S K	2.307	0.03	0.02	0.02	0.83
Mo L	2.293	6.37	0.10	1.15	10.44

*. K the phosphorus and molybdenum lines partially overlap.

Figure 4 shows the micrographs of the SA catalyst samples and S and N distribution maps. The coating is distributed uniformly, and it can be seen that the location areas of S and N coincide. These data are also given in Table 2.

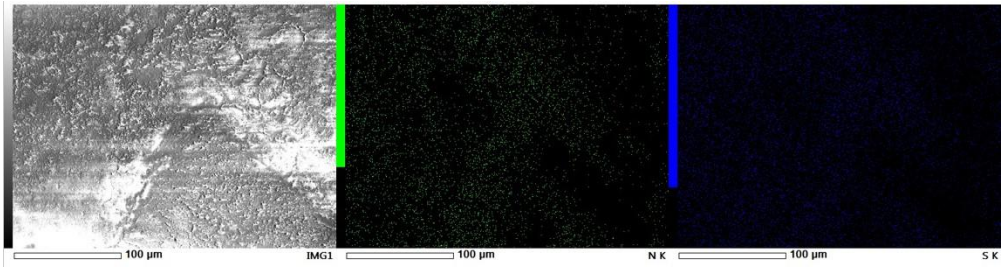

Figure 4. SEM micrograph and distribution of sulfur and nitrogen on the surface of the SA catalyst.

Table 2. Distribution of elements on the SA surface according to EDA data.

Element	(keV)	Weight, %	Sigma	Atom, %	K
C K	0.277	11.09	0.18	23.23	3.06
N K	0.392	3.91	0.24	7.37	4.67
O K	0.525	57.56	0.37	56.22	43.59
Si K	1.739	26.09	0.11	12.00	38.16
S K	2.307	0.54	0.02	0.29	0.83

Figure 5a,b show the nitrogen sorption–desorption curves for the PMo1 and SA catalysts. The hysteresis loop attests to the presence of mesopores.

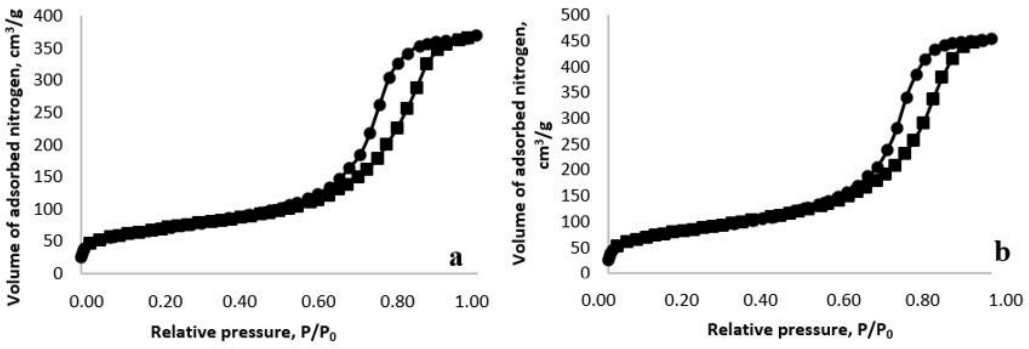

Figure 5. Curve sorption—desorption of nitrogen on the catalyst: (**a**) PMo1, (**b**) SA.

The BJH (Barrett–Joyner–Halenda) average pore diameter and specific volume and the BET (Brunauer–Emmett–Teller) specific surface area for all of the catalysts are summarized

in Table 3. As can be seen, the deposition of the active phase leads to a considerable decrease in the specific surface area and in the pore volume of the PMo1 catalyst, which is caused by the filling and partial blocking of pores. In the case of SA, the average pore diameter markedly decreases, while the specific surface area and the volume of pores barely differ from those of the initial support within the determination error. This difference in the textural characteristics of the two catalysts containing equimolar amounts of the active phase on the surface can be attributed to the large difference between the sizes of the HSO_4^- and $HPMo_{12}O_{40}^{2-}$ anions. Table 3 also presents data from X-ray fluorescence analysis and results of measurements of catalyst acidity by pyridine adsorption.

Table 3. Elemental analysis results, textural characteristics, and catalyst acidity.

Catalyst	*SBET* (m^2/g)	*Dp* (nm)	*Vp* (m^3/g)	Mo, wt.%	BAS *	LAS *
SiO_2	300	10.0	0.75			
PMo1	246	8.6	0.60	9.0	57	17
PMo2	276	9.1	0.62	5.0	88	13
PMo3	291	9.8	0.66	2.4	39	3
SA	297	9.1	0.72		83	0

*—the concentration (A mmol/g) of the Brønsted acid sites (BAS) was determined from the intensity of the adsorbed pyridine band at 1547 cm^{-1}, and the Lewis acid site (LAS) concentration was found from the intensity of the 1450 cm^{-1} band.

As can be seen in Table 3, an increase in the HPA concentration on the surface leads to a monotonic decrease in the pore-specific surface area, volume, and diameter. Meanwhile, as follows from the analysis of the acidity data, the BAS concentration is maximum when the Mo content is medium (PMo2), which corresponds to HPA to betaine molar ratio of 1:3. In this case, the HPA concentration is 45 μmol/g, while the acidity is 88 μmol/g. On going to the PMo1 sample containing a higher concentration of HPA, the acid sites accessible for pyridine adsorption are apparently partially blocked. This is confirmed by the decrease in the pore-specific surface area, volume, and diameter. As a result, for the 80 μmol/g concentration of HPA on the surface, the acidity is only 57 μmol/g. Conversely, a decrease in the molybdenum concentration from 5 to 2.4% (PMo3) leads to a proportional change in the BAS concentration from 88 to 39 μmol/g.

A different picture is observed for LAS: in this case, the concentration of acid sites monotonically decreases with a decrease in the amount of HPA on the surface.

As will be shown below, the highest activity towards the oxidation of sulfur-containing substrates was inherent in the PMo2 catalyst with betaine to HPA ratio of 3:1; therefore, it was studied by X-ray photoelectron spectroscopy.

The survey XPS spectrum of PMo2 (Figure A1a) and high-resolution spectra of the lines of elements (Figures A1b, A2, A3 and A4) were resolved into components corresponding to different states of atoms in the sample (Table 4). The Mo3 XPS spectrum (Figure A3b shows a state with the $Mo3d_{5/2}$ binding energy of 233.2 eV, which can be assigned to molybdenum atoms in the +6 oxidation state. The second state present in the spectrum with the $Mo3d_{5/2}$ binding energy corresponding to 232.0 eV corresponds to Mo^{+5} [38], which apparently appears as a result of the partial reduction of molybdenum during the recording of the spectra. The partial reduction of the sample induced by X-ray radiation is additionally evidenced by a color change (darkening) of the sample at the site exposed to X-rays.

It follows from the analysis of the atomic concentrations of elements in PMo2 (Table 4) that the S:Mo ratio is 3.4, which is somewhat lower than the theoretical value, amounting to 4, while the P:Mo ratio is 6.4, which is also markedly lower than the expected value. The difference between the actual ratios and the theoretical ones may be due to the partial decomposition of HPA during the synthesis to give molybdenum oxides. Because of the smaller size compared to heteropolyanions, molybdenum oxides can diffuse into the inner layer inaccessible for XPS analysis, for example, into the space inside the pores.

Table 4. Element concentrations, binding energies, and fractions of components in XPS spectra, and the corresponding types of bonds in the sample PMo2.

Spectrum	Content Element, at. %	Binding Energies, eV	Fraction, at.%	Type of Chemical Bond
O1s	69.01	530.2 532.8	1.20 67.81	O-Met O-C, SiO_2
N1s	0.52	401.5	0.52	NR_{4+}
$P2p_3/2$	0.12	133.9	0.12	P^{5+}
Si2p	25.24	103.6	25.24	SiO_2
$Mo3d_5/2$	0.77	232.0 233.2	0.42 0.35	Mo^{5+} Mo^{6+}
C1s	4.11	285.0 286.2 287.3 288.8	1.89 1.53 0.54 0.15	C-C C-O, C-N N-C=N, C=O O-C=O
$S2p_3/2$	0.23	168.4	0.23	S6+

The data of the SALDI mass spectrum of the catalyst PMo2 shown in Figure 6 are in line with this conclusion (mass spectra of PMo1 and PMo3 are in Figures A5 and A6). As can be seen, the system with the maximum content of heteropolyacid (PMo1) shows molecular ions, while in the region of low mass, mainly polymeric molybdenum oxides are detected. In the PMo2 and PMo3 catalysts, anions containing less molybdenum than the Keggin structures are present.

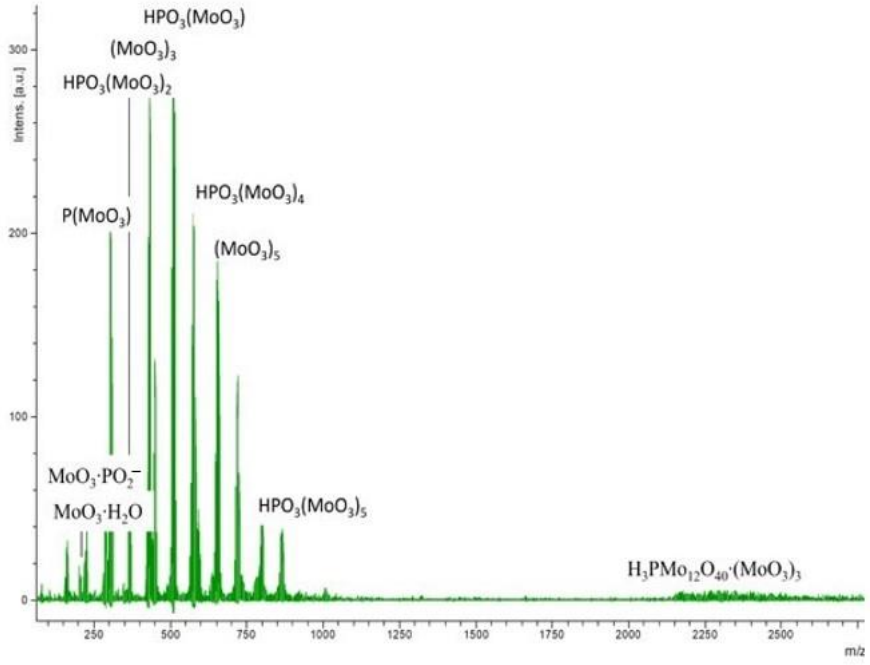

Figure 6. SALDI mass spectra of the PMo2 catalyst in the negative ion detection mode.

According to literature data, these systems often have a catalytic activity higher than the initial heteropolyanions [39].

2.2. Catalytic Properties of Heterogeneous Compositions

Figure 7 shows the time dependence of the degree of removal of thiophene upon oxidation in the presence of the test catalysts and the degree of removal of thiophene in the presence of SA without H_2O_2.

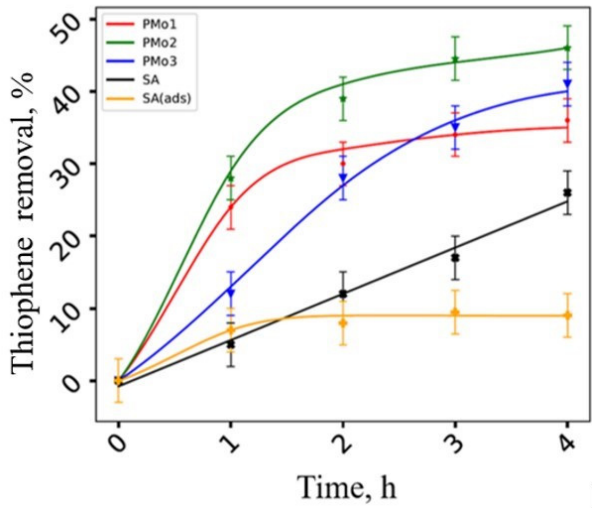

Figure 7. Thiophene removal versus time.

It can be seen that the highest activity towards the oxidation of thiophene is inherent in PMo2. The PMo1 catalyst proved to be less active, despite the higher content of Mo. In the initial part of the curves, the reaction rates are similar; however, subsequently, the reaction catalyzed by the system with a higher metal content is retarded. This trend is attributable to the fact that together with the target reaction, hydrogen peroxide decomposition takes place (Figure 8); this reaction is catalyzed by transition metals, including molybdenum [40].

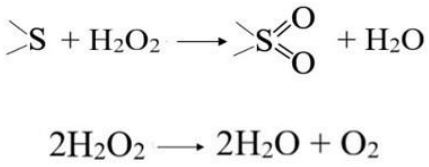

Figure 8. Processes occurring in the system sulfur-containing compound—H_2O_2—catalyst.

Thus, an increase in the molybdenum content on the surface does not lead to a higher activity of the catalyst but, conversely, accelerates the side reaction. Meanwhile, in the case of SA or PMo3 catalysts, that is, when the transition metal is absent or has a low concentration, no retardation of the reaction is observed in the first three hours. The lowest activity was found for SA since Brønsted acids are poor catalysts for thiophene oxidation.

We investigated our systems in three successive cycles of thiophene oxidation. It was found that the SA catalyst is unstable: by the third cycle, the degree of thiophene removal is only 5%. At the same time, molybdenum-based catalysts are more stable: a slight decrease in conversion after the first cycle, which may be associated with the leaching of excess active phase from the surface, is replaced by stable operation of catalysts: thiophene conversions are 34 and 30% for PMo1 and 41 and 40% for PMo2, respectively.

Figures 9 and 10 depict the time dependencies of substrate removal for various catalytic systems. For DBT and pyridine, such as for thiophene, tests were also carried out without hydrogen peroxide to determine the contribution of adsorption to the overall desulfurization.

Analysis of the curves indicates that the above-noted catalyst activity series, PMo2 > PMo1 > PMo3 > SA, holds for sulfur-containing substrates. That is, among the HPA-based catalysts, the catalyst with the highest BAS concentration proved to be the most active. In the case of pyridine, the catalyst activity correlates with the content of HPA on the surface, while the acidity does not significantly affect the removal of pyridine (Figures 10 and 11). This behavior may be due to the fact that, owing to its strong basic properties, pyridine is adsorbed on the acid sites of the catalyst; hence, the catalytic activity is determined only by the content of heteropolyanions. A comparison of the reactivities

of pyridine and sulfur-containing heterocyclic substrates indicates that pyridine is more reactive, especially in the initial stage of the reaction (Figure 11).

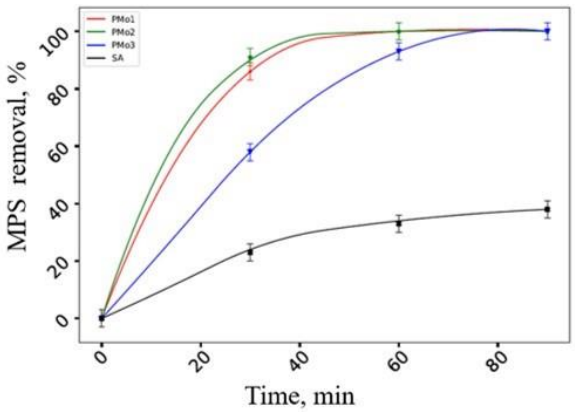

Figure 9. Methylphenyl sulfide (MPS) removal versus time.

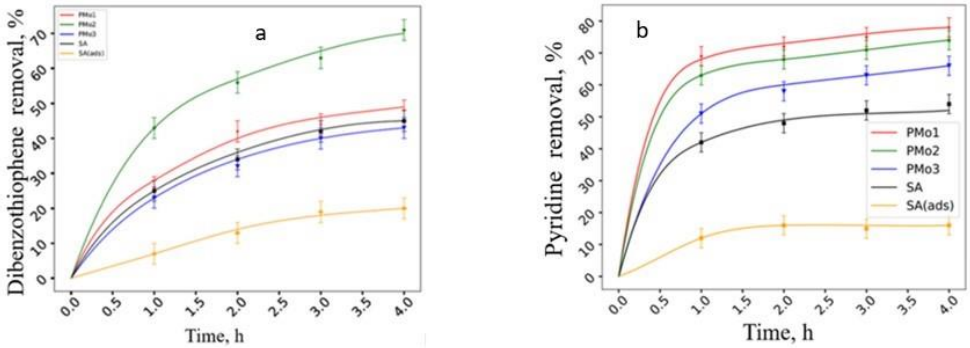

Figure 10. Dibenzothiophene (**a**) and pyridine (**b**) removal versus time.

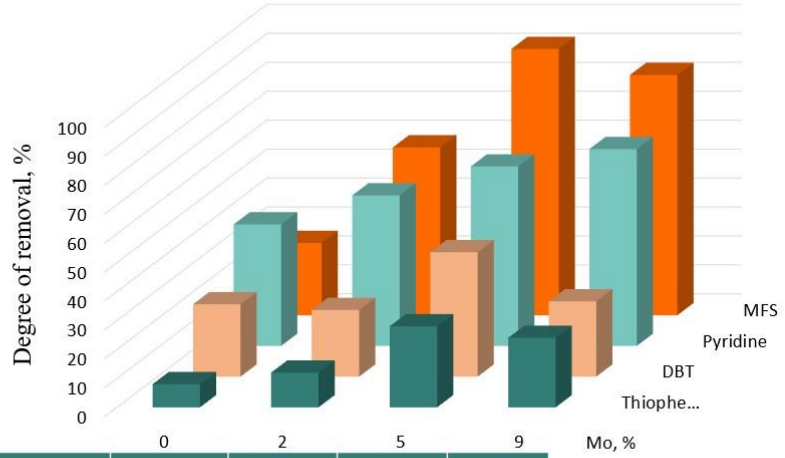

Catalyst	SA	PMo3	PMo2	PMo1
Bronsted acidity (A)	83	39	88	57

Figure 11. Influence of acidity and metal content in catalysts on substrates removal in 1 h (MFS 30 min).

It can be seen in Figure 11 that the acidity affects most appreciably the conversion of dibenzothiophene. In this case, the removal is completely consistent with the acidity series of the catalysts. This might be due to the fact that the presence of an acidic proton disrupts the aromaticity of the dibenzothiophene molecule and thus facilitates the nucleophilic substitution reaction [12,32]. For other sulfur compounds, the influence of both factors (Brønsted acid sites and polyoxymetalate concentration) is quite pronounced.

3. Materials and Methods

3.1. Materials

For the study, we used a BASF Perlkat 97-0 Silica Gel support (as per manufacturer's specifications: specific surface area S = 500 m^2/g; available pore diameter d_p = 10 nm). Sulfuric acid (98%), phosphomolybdic acid (99%) (PMA), isooctane (99.5%), thiophene (99%), dibenzothiophene (99%) (DBT), methylphenyl sulfide (99%) (MFS), pyridine (99%), hydrogen peroxide (30 wt %, high-purity grade) were all purchased from Sigma–Aldrich (Darmstadt, Germany). Betaine, or 4-(3′- ethylimidazolium)-butanesulfonate, was synthesized by the method described in our previous studies [41,42].

3.2. Preparation of Ionic Liquids

For the synthesis of an ionic liquid based on PMA (PMoIL1) 4-(3′-ethylimidazolium)-butanesulfonate (betaine) (0.8 mmol, 0.2 g) was mixed with PMA (≈0.8 mmol, 1.53 g) in a molar ratio of 1:1. The PMA was stirred in 8 mL of H_2O until the heteropolyacid was dissolved. After that, betaine was added, and the mixture was stirred for another 6 h at room temperature. The resulting yellow powder was dried in air.

For the synthesis of an ionic liquid with a reduced content of PMA (PMoIL2), 4-(3′- ethylimidazolium) butanesulfonate (betaine) (0.8 mmol, 0.2 g) was mixed with PMA (≈0.3 mmol, 0.49 g) in a molar ratio of 3:1 in 5 ml of H_2O and the procedure was carried out in the same way.

For the synthesis of an ionic liquid based on sulfuric acid (SAIL), betaine (0.5 mmol, 1.2 g) was mixed with sulfuric acid (0.5 mmol, 0.5 mL) in a 1:1 molar ratio. The mixture was stirred for 24 h at 70 °C, after which it was washed three times with diethyl ether (3 × 15 mL).

3.3. Preparation of Catalysts

To obtain a heterogeneous PMo1 catalyst, 10 mL of H_2O was added to 1.8 g of PMoIL1 and stirred until dissolved. Then, 4.79 g of SiO_2 was added and the mixture was stirred at room temperature for 13 h. The excess solvent was removed in a stream of air at room temperature and then by heating to 40 °C for 6 h. During the reaction, the IL partially decomposed with MoO_3 formation. Therefore, the molybdenum concentration on the surface turned out to be less than the calculated one.

To obtain a heterogeneous catalyst with a possible assignment of PMA (PMo2), 10 mL of H_2O was added to 0.69 g of PMoIL2 and changed until dissolved. Then, 4.8 g of silica gel was added, and the mixture was stirred at room temperature for 13 h. In this case, IL was completely adsorbed on the support.

The PMo3 catalyst was obtained without preliminary isolation of the corresponding IL. For this, PMA (0.1 g, 0.06 mmol) was dissolved in 5 mL of water, and then 0.1 g (0.4 mmol) of betaine was added. After the resulting mixture was dissolved, 2.3 g of silica gel was added, and the solution was stirred for 6 h at 40 °C. Next, the solvent was removed similarly to the previous experiment.

To prepare the SA catalyst, 0.2 g of SAIL was dissolved in 10 mL of water, then 3.9 g of silica gel was added, and the mixture was stirred for 5 h at room temperature. The solvent was removed in a stream of air and dried at 50 °C. Thus, the content of the active phase is about 5 wt.%.

3.4. Methods for the Analysis of Ionic Liquids and Catalysts

IR spectra in KBr pellets were recorded on an Infralum FT-801 FT-IR spectrophotometer (LLC Lumex-Siberia, Novosibirsk, Russia) in the range of 4000–400 cm^{-1}.

The concentration of acid sites in the samples was determined using IR spectroscopy of adsorbed pyridine from the intensity of the adsorbed pyridine band at 1547 and 1450 cm^{-1}. The extinction coefficient from work was used in the calculations [43].

The surface of the catalysts was examined by scanning electron microscopy (JEOL Ltd, Tokyo, Japan). To achieve this, we used a JEOL JSM-6000 NeoScope electron microscope with a built-in EX-230 X-ray analyzer for energy-dispersive analysis of particle distribution.

Adsorption measurements were carried out on an ASAP 20000N Micromeritics automatic sorptometer (Micromeritics, Norcross, GA, USA).

For the determination of molybdenum in synthesized samples, the high-aperture sequential X-ray fluorescence wavelength-dispersive spectrometer SPECTROSCAN MAX-G (SPECTRON, St. Petersburg, Russia) was used [30]. The determination was carried out according to the line MoK_a (70.9 pm) by the method of an external standard (usual calibration). The composition of heteropolyanions on the surface of the catalysts was determined by mass spectrometry using the SALDI technique (surface-activated laser desorption/ionization).

The mass spectra of the samples were recorded in the RN Pep Mix mode on a Bruker Ultra-flex instrument equipped with a nitrogen laser, and a time-of-flight mass analyzer. The spectra were recorded using a reflectron in the negative ion registration mode. Identification of cluster ions by isotopic distribution was carried out using the IsoPro simulator program.

X-ray photoelectron spectra of the PMo2 catalyst were recorded on an Axis Ultra DLD spectrometer (Kratos) using monochromatic AlKa radiation with a neutralizer.

3.5. Catalytic Test

For the oxidation of sulfur-containing compounds with hydrogen peroxide, a model mixture in an amount of 10 mL (1 wt % of thiophene, dibenzothiophene, methylphenylsulfide or pyridine in isooctane), as well as a catalyst (0.1 g) and an oxidizer (H_2O_2, 0.4 mL) were placed in a jacketed reactor with a magnetic stirrer.

The contents of the reactor were stirred while heating (60 °C), and samples of the organic phase were periodically taken for analysis by gas–liquid chromatography on a Kristall-2000 instrument (Chromatec, Yoshkar-Ola, Russia) with a Zebron ZB-1 (Phenomenex Inc, Torrance, CA, USA) capillary column (30 m) and a flame ionization detector.

The determination of the conversion of substrates was established by the decrease in their content in the organic phase of their data GLC by the method of internal standard, which was used as nonane or dodecane.

To carry out experiments to determine the stability of the catalysts in successive cycles, after the completion of the reaction, the liquid phase was poured out, a new portion of the reagents was placed in the reactor, and the tests were carried out in a similar way.

To evaluate the contribution of adsorption to the total degree of removal of heteroatomic substrates for thiophene DBT and pyridine, we also performed a series of experiments on the SA catalyst, similar to those described above, but without the addition of an oxidizing agent.

4. Conclusions

A series of effective catalysts for the oxidation of sulfur and nitrogen compounds were obtained using betaine and sulfuric or phosphomolybdic acids with different contents of the active phase on the support surface. Apart from the catalytic properties, the catalysts combine extractant and adsorbent functions. It was shown that an increase in the amount of heteropolyacid induces a non-linear variation of the acidity: the highest concentration of Brønsted acid sites is observed for a catalyst with a medium content of the heteropolyacid. The conversion of dibenzothiophene is correlated with the concentration of Brønsted acid sites on the surface. In the case of pyridine, the degree of removal is determined, first of all, by the content of the heteropolyacid in the catalyst because the substrate, which is basic, can block the acid-active sites. For other sulfur-containing substrates, both characteristics of the catalyst are significant.

Author Contributions: Conceptualization, I.T.; methodology, I.T.; software, A.G.P.; validation, I.T.; formal analysis, A.B., K.O. and A.G.P.; investigation, I.T. and V.G.; resources, V.G.; data curation, V.G.; writing—original draft preparation, V.G. and I.T.; writing—review and editing, V.G., I.T., A.B. and K.O.; visualization, V.G.; supervision, I.T.; project administration, I.T.; funding acquisition, I.T. All authors have read and agreed to the published version of the manuscript.

Funding: This research received no external funding.

Data Availability Statement: Data is contained within the article.

Acknowledgments: This work was carried out within the framework of the Lomonosov Moscow State University State order (project no. AAAA-A21-121011590090) using equipment purchased with funds from the Lomonosov Moscow State University development program.

Conflicts of Interest: The authors declare no conflict of interest. The funders had no role in the design of the study.

Appendix A. XPS and SALDI Spectrums

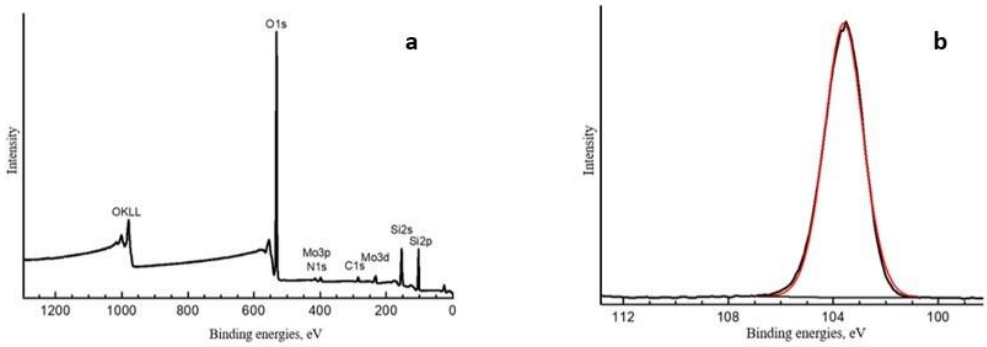

Figure A1. Panoramic (**a**) and Si2p (**b**) XPS spectrum of the test sample.

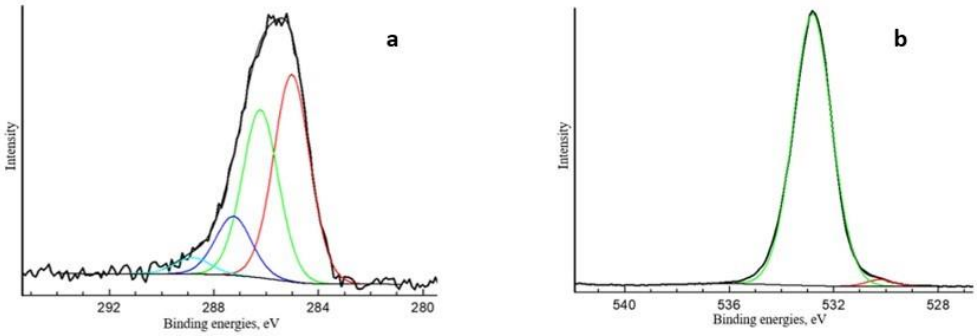

Figure A2. C1s (**a**) and O1s (**b**) XPS spectrum of the test sample.

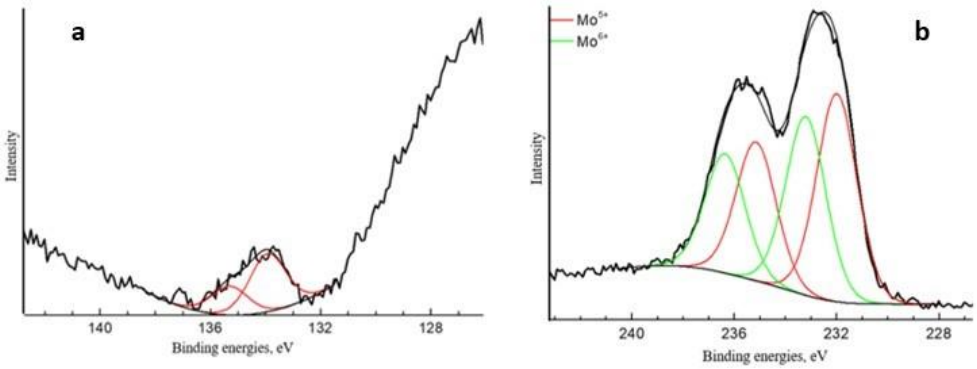

Figure A3. P2p (**a**) and Mo3d (**b**) XPS spectrum of the test sample.

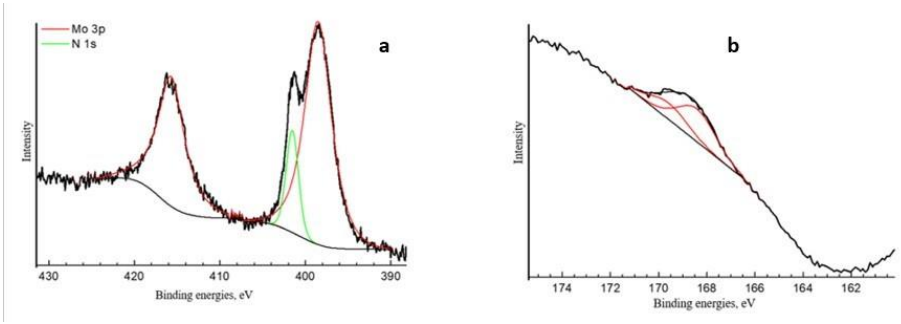

Figure A4. Mo3p/N1s (**a**) and S2p (**b**) XPS spectrum of the test sample.

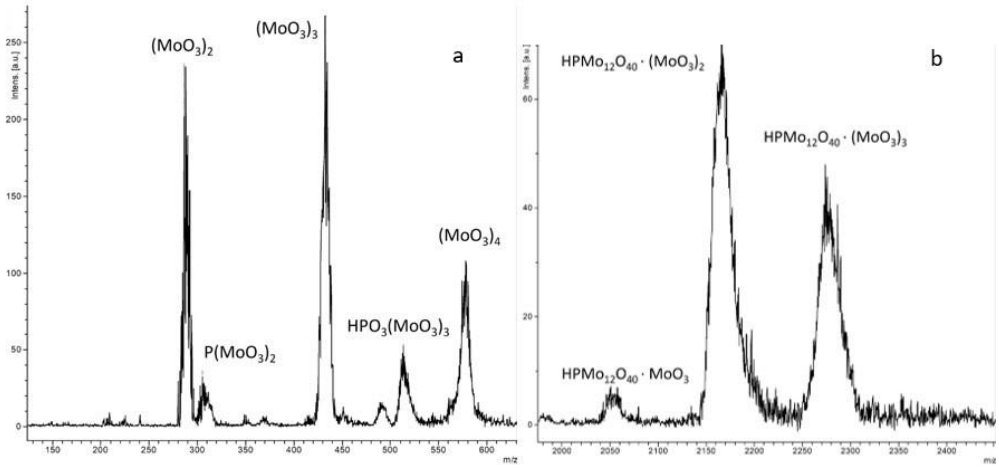

Figure A5. SALDI mass spectra of the PMo1 catalyst—in the region of low (**a**) and high (**b**) masses in the negative ion detection protocol.

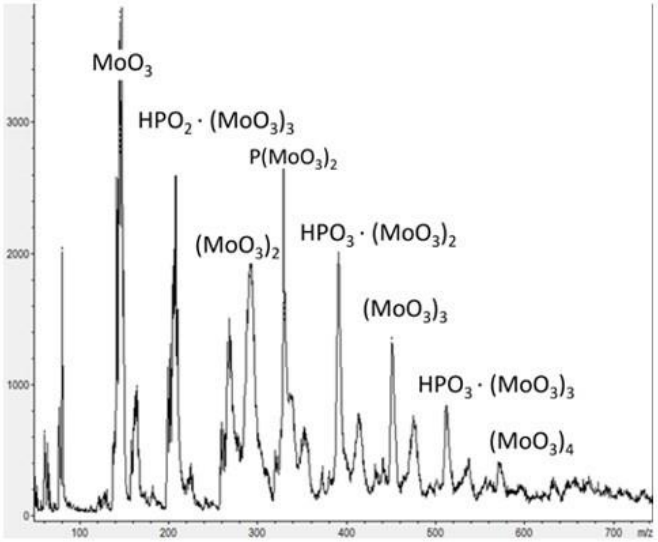

Figure A6. SALDI mass spectra of the PMo3 catalyst in the negative ion detection mode.

References

1. Koolen, C.D.; Rothenberg, G. Air Pollution in Europe. *ChemSusChem* **2019**, *12*, 164–172. [CrossRef]
2. Cui, T.; Fan, H.; Yang, Z.; Feng, J.; Li, W. A comprehensive review on oxidative desulfurization catalysts targeting clean energy and environment. *J. Mater. Chem. A* **2020**, *8*, 2246–2285.
3. Yang, L.; Franco, V.; Mock, P.; Kolke, R.; Zhang, S.; Wu, Y.; German, J. Experimental Assessment of NO x Emissions from 73 Euro 6 Diesel Passenger Cars. *Environ. Sci. Technol.* **2015**, *49*, 14409–14415. [CrossRef]

4. Yang, Q.; Wang, Y.; Tang, X.; Zhang, Q.; Dai, S.; Peng, H.; Lin, Y.; Tian, Z.; Lu, Z.; Chen, L. Ligand Defect Density Regulation in Metal–Organic Frameworks by Functional Group Engineering on Linkers. *Nano Lett.* **2022**, *22*, 838–845. [CrossRef] [PubMed]
5. Abro, R.; Abro, M.; Gao, S.; Bhutto, A.W.; Ali, Z.M.; Shah, A.; Chen, X.; Yu, G. Extractive Denitrogenation of Fuel Oils Using Ionic Liquids: A Review. *RSC Adv.* **2016**, *6*, 93932–93946. [CrossRef]
6. Glotov, A.P.; Vutolkina, A.V.; Vinogradov, N.A.; Pimerzin, A.A.; Vinokurov, V.A.; Pimerzin, A.A. Enhanced HDS and HYD Activity of Sulfide Co-PMo Catalyst Supported on Alumina and Structured Mesoporous Silica Composite. *Catal. Today* **2021**, *377*, 82–91. [CrossRef]
7. Tanimu, A.; Alhooshani, K. Advanced Hydrodesulfurization Catalysts: A Review of Design and Synthesis. *Energy Fuels* **2019**, *33*, 2810–2838. [CrossRef]
8. Liu, F.; Yu, J.; Qazi, A.B.; Zhang, L.; Liu, X. Metal-Based Ionic Liquids in Oxidative Desulfurization: A Critical Review. *Environ. Sci. Technol.* **2021**, *55*, 1419–1435. [CrossRef]
9. Houda, S.; Lancelot, C.; Blanchard, P.; Poinel, L.; Lamonier, C. Oxidative Desulfurization of Heavy Oils with High Sulfur Content: A Review. *Catalysts* **2018**, *8*, 344. [CrossRef]
10. Ahmadian, M.; Anbia, M. Highly efficient oxidative desulfurization catalyzed by copper-based materials using hydrogen peroxide as oxidant. *Fuel* **2022**, *324*, 124471. [CrossRef]
11. Ma, S.; Bao, W.; Liu, B.; Zhang, C.; Wang, C.; Liu, Y.; Guo, P. Mo11V polyoxometalate encapsulated into hollow mesoporous carbon spheres: A highly efficient and ultrastable catalyst for oxidative desulfurization. *Appl. Surf. Sci.* **2022**, *606*, 154781. [CrossRef]
12. Bryzhin, A.A.; Gantman, M.G.; Buryak, A.K.; Tarkhanova, I.G. Brønsted Acidic SILP-Based Catalysts with H3PMo12O40 or 334 H3PW12O40 in the Oxidative Desulfurization of Fuels. *Appl. Catal. B Environ.* **2019**, *257*, 117938. [CrossRef]
13. Kumar, S.; Chandra Srivastava, V.; Kumar, A.; Nanoti, S.M. Effect of Gas Oil Composition on Performance Parameters of the Extractive Desulfurization Process. *RSC Adv.* **2016**, *6*, 25293–25301. [CrossRef]
14. Valenzuela, C.; Donoso, C.; Guzmán-Beckmann, L. Extraction of Sulfur from Commercial Gasoline Using 1-Butyl-3-Methylimidazolium Tetrafluoroborate [BMIM] [BF4] as the Extraction Solvent. *Key Eng. Mater.* **2020**, *834*, 42–48. [CrossRef]
15. Ahmed, O.U.; Mjalli, F.S.; Talal, A.-W.; Al-Wahaibi, Y.; Al Nashef, I.M. Extractive Desulfurization of Liquid Fuel Using Modified Pyrollidinium and Phosphonium Based Ionic Liquid Solvents. *J. Solut. Chem.* **2018**, *47*, 468–483. [CrossRef]
16. Aslam, S.; Subhan, F.; Yan, Z.; Etim, U.J.; Zeng, J. Dispersion of Nickel Nanoparticles in the Cages of Metal-Organic Framework: An Efficient Sorbent for Adsorptive Removal of Thiophene. *Chem. Eng. J.* **2017**, *315*, 469–480. [CrossRef]
17. Zhao, Z.; Zuhra, Z.; Qin, L.; Zhou, Y.; Zhang, L.; Tang, F.; Mu, C. Confinement of Microporous MOF-74(Ni) within Mesoporous y-Al2O3 Beads for Excellent Ultra-Deep and Selective Adsorptive Desulfurization Performance. *Fuel Process. Technol.* **2018**, 276–282. [CrossRef]
18. Wang, S.; Tong, H.; Li, H.; Shi, X.; Liu, D.; Li, J.; Guo, K.; Zhao, L.; Song, S.; Chen, L.; et al. Synthesis of a Phosphomolybdic Acid/Nanocrystalline Titanium Silicalite-1 Catalyst in the Presence of Hydrogen Peroxide for Effective Adsorption-Oxidative Desulfurization. *New J. Chem.* **2022**, *46*, 2559–2568. [CrossRef]
19. Vafaee, F.; Mandizadeh, S.; Amiri, O.; Jahangiri, M.; Salavati-Niasari, M. Correction: Synthesis and Characterization of AFe2O4 (A: Ni, Co, Mg)–Silica Nanocomposites and Their Application for the Removal of Dibenzothiophene (DBT) by an Adsorption Process: Kinetics, Isotherms and Experimental Design. *RSC Adv.* **2022**, *12*, 20973–20974. [CrossRef] [PubMed]
20. Crandall, B.S.; Zhang, J.; Stavila, V.; Allendorf, M.D.; Li, Z. Desulfurization of Liquid Hydrocarbon Fuels with Microporous and Mesoporous Materials: Metal-Organic Frameworks, Zeolites, and Mesoporous Silicas. *Ind. Eng. Chem. Res.* **2019**, *58*, 19322–19352. [CrossRef]
21. Khudoyarova, O.; Gordienko, O.; Sydoruk, T.; Titov, T.; Petruk, R.; Prokopchuk, S. Adsorptive desulfurization of industrial wastewater. *Environ. Probl.* **2020**, *5*, 102–105. [CrossRef]
22. Singh, S.K.; Savoy, A.W. Ionic Liquids Synthesis and Applications: An Overview. *J. Mol. Liq.* **2020**, *297*, 112038. [CrossRef]
23. Moreno, D.; Gonzalez-Miquel, M.; Ferro, V.R.; Palomar, J. Molecular and Thermodynamic Properties of Zwitterions versus Ionic Liquids: A Comprehensive Computational Analysis to Develop Advanced Separation Processes. *ChemPhysChem* **2018**, *19*, 794. [CrossRef]
24. Hatab, F.A.; Darwish, A.S.; Lemaoui, T.; Warrag, S.E.E.; Benguerba, Y.; Kroon, M.C.; AlNashef, I.M. Extraction of Thiophene, Pyridine, and Toluene from n-Decane as a Diesel Model Using Betaine-Based Natural Deep Eutectic Solvents. *J. Chem. Eng. Data* **2020**, *65*, 5443–5457. [CrossRef]
25. Hao, Y.; Hao, Y.; Ren, J.; Wu, B.; Wang, X.; Zhao, D.; Li, F. Extractive/Catalytic Oxidative Mechanisms over [Hnmp]ClxFeCl3 Ionic Liquids towards the Desulfurization of Model Oils. *New J. Chem.* **2019**, *43*, 7725–7732. [CrossRef]
26. Chen, L.; Wang, J.A.; de la Fuente, N.; Zhou, S.; Jiang, P.; Song, Y.; Zhou, X. Roles of the Structural Defects and the Combined Acidity of H 3 PW 12 O 40 /Zr-MCM-41 Catalysts in Ultralow Sulfur Diesel Production. *New J. Chem.* **2022**, *46*, 2081–2093. [CrossRef]
27. Vafaeezadeh, M.; Alinezhad, H. Brønsted Acidic Ionic Liquids: Green Catalysts for Essential Organic Reactions. *J. Mol. Liq.* **2016**, *218*, 95–105. [CrossRef]
28. Ibrahim, M.H.; Hayyan, M.; Hashim, M.A.; Hayyan, A. The Role of Ionic Liquids in Desulfurization of Fuels: A Review. *Renew. Sustain. Energy Rev.* **2017**, *76*, 1534–1549. [CrossRef]
29. Mai, N.L.; Ahn, K.; Koo, Y.-M. Methods for Recovery of Ionic Liquids—A Review. *Process Biochem.* **2014**, *49*, 872–881. [CrossRef]

30. Ali-Zade, A.G.; Buryak, A.K.; Zelikman, V.M.; Oskolok, K.V.; Tarkhanova, I.G. SILCs in Oxidative Desulfurization: Effect of Support and Heteropolyanion. *New J. Chem.* **2020**, *44*, 6402–6410. [CrossRef]
31. Gorbunov, V.S.; Bryzhin, A.A.; Popov, A.G.; Tarkhanova, I.G. Immobilized Acid Catalysts in the Oxidation of Sulfur-Containing Compounds with Hydrogen Peroxide. *Pet. Chem.* **2021**, *61*, 1260–1269. [CrossRef]
32. Akopyan, A.; Eseva, E.; Polikarpova, P.; Kedalo, A.; Vutolkina, A.; Glotov, A. Deep Oxidative Desulfurization of Fuels in the Presence of Brönsted Acidic Polyoxometalate-Based Ionic Liquids. *Molecules* **2020**, *25*, 536. [CrossRef]
33. Prado, G.H.C.; Rao, Y.; de Klerk, A. Nitrogen Removal from Oil: A Review. *Energy Fuels* **2017**, *31*, 14–36. [CrossRef]
34. Julião, D.; Gomes, A.C.; Pillinger, M.; Gonçalves, I.S.; Balula, S.S. Desulfurization and Denitrogenation Processes to Treat Diesel 388 Using Mo(VI)-Bipyridine Catalysts. *Chem. Eng. Technol.* **2020**, *43*, 1774–1783. [CrossRef]
35. Zhu, X.; Liu, M.; Liu, Z.; Li, Y.; Tian, S. Direct and Rapid Quantitative Analysis of Alkyldibenzothiophenes in Deeply Hy- 390 drodesulfurized Diesel Fuel by Gas Chromatography Quadrupole Time-of-Flight Mass Spectrometry. *Energy Fuels* **2017**, *31*, 9125–9131. [CrossRef]
36. Rocchiccioli-Deltcheff, C.; Aouissi, A.; Bettahar, M.; Launay, S.; Fournier, M. Catalysis by 12-Molybdophosphates. *J. Catal.* **1996**, *164*, 16–27. [CrossRef]
37. Langer, R.; Phys, J. FT-IR investigation of polarizable, strong hydrogen bonds in sulfonic acid-sulfoxide, phosphine oxide, and arsine oxide complexes in the middle and far-infrared region. *J. Phys. Chem.* **1995**, *99*, 12214–12219. [CrossRef]
38. Baltrusaitis, J.; Mendoza-Sanchez, B.; Fernandez, V.; Veenstra, R.; Dukstiene, N.; Roberts, A.; Fairley, N. Generalized Molybdenum Oxide Surface Chemical State XPS Determination via Informed Amorphous Sample Model. *Appl. Surf. Sci.* **2015**, *326*, 151–161. [CrossRef]
39. Kozhevnikov, I. Catalysts for Fine Chemical Synthesis. In *Catalysis by Polyoxometalates 2*; 2002; Volume 2, p. 220. Wiley: Hoboken, NJ, USA.
40. Smolin, R.A. Catalytic Peroxide Decomposition of a Publicly Available Oxo-Peroxo Molybdenum Compound. *Bull. Kazan Technol. Univ.* **2011**, *15*, 57–61.
41. Tarkhanova, I.G.; Bryzhin, A.A.; Gantman, M.G.; Yarovaya, T.P.; Lukiyanchuk, I.V.; Nedozorov, P.M.; Rudnev, V.S. Ce-, Zr-Containing Oxide Layers Formed by Plasma Electrolytic Oxidation on Titanium as Catalysts for Oxidative Desulfurization. *Surf. Coat. Technol.* **2019**, *362*, 132–140. [CrossRef]
42. Bryzhin, A.A.; Tarkhanova, I.G.; Gantman, M.G.; Rudnev, V.S.; Vasilyeva, M.S.; Lukiyanchuk, I.V. Titanium-Supported W-Containing PEO Layers Enriched with Mn or Zn in Oxidative Desulfurization and the Zwitterionic Liquid Effect. *Surf. Coat. Technol.* **2020**, *393*, 125746. [CrossRef]
43. Tamura, M.; Shimizu, K.; Satsuma, A. Comprehensive IR Study on Acid/Base Properties of Metal Oxides. *Appl. Catal. A Gen.* **2012**, *433–434*, 135–145. [CrossRef]